Toxicology Letters 229 (2014) 167–177

Contents lists available at ScienceDirect

Toxicology Letters

journal homepage: www.elsevier.com/locate/toxlet

Toxic response of HIPCO single-walled carbon nanotubes in mice and RAW264.7 macrophage cells

Eun-Jung Park [a,*], Nur Elida M. Zahari [a], Min-Sung Kang [b], Sang jin Lee [b], Kyuhong Lee [b], Byoung-Seok Lee [c], Cheolho Yoon [d], Myung-Haing Cho [e], Younghun Kim [f], Jae-Ho Kim [a,**]

[a] Department of Molecular Science and Technology, Ajou University, Suwon 443-749, Republic of Korea
[b] Inhalation Toxicology Center, Korea Institute of Toxicology, Jeongeup 580-185, Republic of Korea
[c] Toxicologic Pathology Center, Korea Institute of Toxicology, Daejeon, Republic of Korea
[d] Seoul Center, Korea Basic Science Institute, Seoul 126-16, Republic of Korea
[e] College of Veterinary Medicine, Seoul National University, Seoul 151-742, Republic of Korea
[f] Department of Chemical Engineering, Kwangwoon University, Seoul 139-701, Republic of Korea

HIGHLIGHTS

- We identified an innate immune toxic response of SWCNT synthesized by HIPCO method.
- In mice, the number of total cells and the secretion of IL-6 and MCP-1 increased.
- The portion of neutrophils, lymphocytes, and eosinophils increased.
- In RAW264.7 cells, cell viability and ATP production decreased.
- The levels of apoptosis-, autophagy- and ER stress-related proteins increased.
- Autophagosome, the ER dilatation and mitochondrial flocculent densities were observed.

ARTICLE INFO

Article history:
Received 8 April 2014
Received in revised form 6 June 2014
Accepted 7 June 2014
Available online 11 June 2014

Keywords:
SWCNT
Macrophages
Apoptosis
Autophagy
Mitochondria
ER stress

ABSTRACT

In this study, we identified the toxic response of pristine single-walled carbon nanotubes (P-SWCNTs) synthesized by HIPCO method in mice and RAW264.7 cells, a murine peritoneal macrophage cell line. P-SWCNT contained a large amount of Fe ion (36 wt%). In the lungs of mice 24 h after intratracheal administration, P-SWCNTs increased the secretion of IL-6 and MCP-1, and the number of total cells, the portion of neutrophils, lymphocytes, and eosinophils, also significantly increased at a 100 μg/mL of concentration. In RAW264.7 cells, cell viability and ATP production decreased in a dose-dependent manner at 24 h after exposure, whereas the generations of ROS and NO were enhanced at all concentrations together with the activation of the MAP kinase pathway. Moreover, the levels of both apoptosis- and autophagy-related proteins and ER stress-related proteins clearly increased, and the concentrations of Fe, Cu, and Zn ions, but not of Mn ions, increased in a dose-dependent manner. TEM images also revealed that P-SWCNTs induced the formation of autophagosome-like vacuoles, the dilatation of the ER, the generation of mitochondrial flocculent densities, and the separation of organelle by disappearance of the cell membrane. Taken together, we suggest that P-SWCNTs cause acute inflammatory response in the lungs of mice, and induce autophagy accompanied with apoptosis through mitochondrial dysfunction and ER stress in RAW264.7 cells. Furthermore, further study is required to elucidate how the physicochemical properties of SWCNTs determine the cell death pathway and an immune response.

1. Introduction

Single-walled CNTs (SWCNTs) are used in a wide spectrum of applications, including dent-resistant car bodies, earthquake-resistant buildings, stain-resistant textiles, nanowires, semiconductors, transistors, chemical sensors, biomedical imaging systems, and

* Corresponding author. Tel.: +82 31 219 3332; fax: +82 31 219 3331.
** Corresponding author. Tel.: +82 31 219 2517; fax: +82 31 219 2516.
E-mail addresses: pejtoxic@hanmail.net (E.-J. Park), jhkim@ajou.ac.kr (J.-H. Kim).

http://dx.doi.org/10.1016/j.toxlet.2014.06.015
0378-4274/

drug- and gene-delivery systems (Arlt et al., 2010; de la Zerda et al., 2011; Lamm and Ke 2010; Prato et al., 2008; Saito et al., 2009; Usui et al., 2008). Conversely, SWCNTs, which are constructed featuring a high length-to-diameter ratio, have continued to raise safety concerns because of their potentially harmful health effects (Lam et al., 2006; Gulati and Gupta 2012; Boczkowski and Lanone 2012; Manke et al., 2013).

SWCNTs can be synthesized using different methods including arc discharge, laser ablation, chemical vapor deposition (CVD) from hydrocarbons and high pressure conversion of carbon monoxide (HIPCO), and the properties of SWCNTs including purities, lengths, chiralities, diameters, and graphitization grades, can be different depending on these synthetic methods (Rösner et al., 2014). The primary properties of nanomaterials produced in synthetic or manufacturing processes are key factors that determine toxicity and the mechanism of nanomaterials together with the properties of biological systems used in experiments. Moreover, the primary properties of nanomaterials are readily altered not only within biocompatible vehicles that are used in toxicity tests but also within the biological system. Therefore, various factors must be considered concurrently to accurately interpret the results obtained from toxicity tests (Nel et al., 2009; Walkey and Chan, 2012; Saptarshi et al., 2013). For example, SWCNTs synthesized by CVD method (Fe content, approximately 0.81 wt%) did not decrease cell viability in RAW264.7 cells, a murine peritoneal macrophage cell line, up to the concentration of 50 μg/mL, whereas their acid-functionalization (iron (Fe) content, 0.056 wt%) induced 4.7 and 15% losses of cell viability at concentrations of 10 and 50 μg/mL, respectively (Dong et al., 2012). In addition, SWCNTs (Fe content, <35 wt%) synthesized by HIPCO method induced relatively high toxicity in BEAS-2B cells, a human bronchial epithelial cell line (Park et al., 2014a). Also, Kagan et al. (2006) reported that SWCNTs (Fe content, 26 wt%) synthesized by HIPCO method caused accumulation of lipid peroxidation and loss of intracellular glutathione in RAW264.7 cells, and their acid treatment (Fe content, 0.23 wt%) was effective for reduction of oxidative stress. Furthermore, although SWCNTs were synthesized by the same method (electric arc discharge method), SWCNTs functionalized by carboxylic acid only among different three groups, carboxylic acid, polyaminobenzene sulfonic acid, and polyethylene glycol, induced autophagic cell death (Liu et al., 2011). Additionally, the surface charge of SWCNTs influences mutual interaction between SWCNT surfaces, surfactants, and solvents, and toxicity of SWCNTs can be reduced by biocompatible nanoscale dispersion (Mutlu et al., 2010).

Recently, some researchers have suggested that SWCNTs induce not only apoptotic but also autophagic cell death *in vitro* (Wang et al., 2012; Liu et al., 2011; Dong et al., 2012; Wan et al., 2013; Witasp et al., 2009; Ma et al., 2012), but mechanistic data on the toxicity of SWCNTs still lack. Also, in our previous study, we identified immune responses of SWCNTs synthesized by arc-discharge process (Park et al., 2011a,b). Therefore, in this study, we characterized pristine SWCNTs synthesized by HIPCO method (P-SWCNT), and then identified their toxicity and the mechanism in mice and RAW264.7 cells.

2. Materials and methods

2.1. Preparation and characterization of P-SWCNT

P-SWCNT (Fe content, <35 wt%) was purchased from Unidym (Sunnyvale, CA, USA), and dispersed in phosphate-buffered saline (PBS, 0.15 M, pH 7.2, Ca^{2+}- and Mg^{2+}-free) containing 0.5% Pluronic F127 as described previously (Park et al., 2014a, Supple 1). The final concentrations of P-SWCNT and Fe in the dispersion were 14.58 μg/mL and 8.396 ppm, respectively, and thus, the weight composition of Fe was 36% in the dispersed P-SWCNT, which is similar to that in raw materials. Table 1 summarizes characterization of P-SWCNT. Moreover, culture media (500 μL/sample) in the absence or the presence of P-SWCNT were digested in a mixed solution of HNO_3 (70%) and H_2O_2 (30%) by using a microwave digestion system (Milestone, Sorisole, Italy) under high temperature and pressure, and the Fe concentrations in lysates were determined using inductively coupled plasma (ICP)-mass spectrometry (MS, 7700, Agilent, Japan) in Korean Basic Science Institute (Seoul, Korea). They were 0.40 ± 0.01 ppm, 0.66 ± 0.03 ppm, 1.20 ± 0.03 ppm, and 2.23 ± 0.06 ppm at 0.8, 1.7, 3.3, and 6.6 μg/mL of P-SWCNT, respectively, and that in medium containing vehicle only was 0.11 ± 0.00 ppm (data not shown).

2.2. In vivo sample preparation

Five-week-old male ICR mice (25–26 g, OrientBio, Seongnam, Korea) were acclimatized for 1 week before the start of the study at a constant temperature of 23 ± 3 °C, with relative humidity of 50 ± 10%, a 12-h light/dark cycle with a light of intensity of 150–300 lux, and ventilation of 10–20 times per hour. Temperature and relative humidity were monitored and recorded daily. For comparison with our previous studies (Park et al., 2011a,b), P-SWCNT was delivered using a 24-gauge catheter at a dose of 25, 50 and 100 μg/kg by intratracheal administration under light tiletamine anesthesia. The control group was treated with PBS containing 0.5% Pluronic F127. At 24 h after administration, bronchoalveolar lavage (BAL) fluids were obtained by cannulating the trachea and lavaging the lungs with 1 mL of cold sterile PBS. Approximately 500–600 μL of BAL fluid per mouse was harvested and centrifuged at 3000 rpm for 10 min. Cell pellets and supernatants were used for BAL fluid cells and cytokine analysis, respectively. The experiments were assessed by the Institutional Animal Care and Committee (IACUC) of Ajou University (Suwon, Korea, IACUC No. 2012-0010) and Korea Institute of Toxicology (Jeongup, Korea, 14-0-0076) and performed in accordance with the "Guide for the Care and Use of Laboratory Animals", an ILAR publication.

2.3. BAL fluid analysis

The number of total cells in BAL fluid was recorded using automatic cell counter (ViCell XR, Beckman Coulter, CA, USA). And, cytospinning was performed with 500 μL BAL fluid harvested at 24 h after a single administration. After cytospinning, slides were fixed in methanol and stained with Diff-Quick (Sysmex Corporation, Tokyo, Japan), and different cell types in the BAL fluid were quantified by their characteristic morphologies.

2.4. Cytokine analysis

To measure changes in the levels of innate immune response-related cytokines, including interleukine (IL)-1β, tumor necrosis factor alpha (TNFα), monocyte chemotactic protein (MCP)-1 and IL-6, we used commercially available enzyme-linked immunosorbent assay (ELISA) kits (eBioscience) (Park et al., 2011a,b). Briefly, each well in the microplates was coated with capture antibody and

Table 1
A summary of characterization of P-SWCNT in vehicles.

Solution	Surface charge (mV)	Hydrodynamic size (nm)
Vehicle	1.2 ± 3.4	135.5 ± 23.1
Cell culture media	1.8 ± 4.8	91.3 ± 12.3
Gamble's solution	4.0 ± 0.8	143.6 ± 3.5

incubated overnight at 4 °C. After washing, each well was blocked with assay diluent, samples and standard antibody were added to the individual wells, and the plates were then maintained at room temperature (RT) for 2 h. Next, biotin-conjugated detecting antibody was added to each well, and the plates were put at RT for 1 h. The reactants were further incubated with avidin-horseradish peroxidase for 30 min. Finally, the reactions were stopped by adding 1 M H_3PO_4, and absorbance was measured at 450 nm with an ELISA plate reader (VersaMax, Molecular Devices, Sunnyvale, CA, USA). The amount of cytokine was calculated from the linear portion of the standard curve which was produced in the same condition.

2.5. Histopathological analysis

Lung tissues were harvested from four mice per group, and fixed with 10% neutral buffered formalin. Histopathological analysis was performed at the Korea Institute of Toxicology (Daejeon, Korea) according to standard operating procedure.

2.6. Cell culture

RAW264.7 cells, which are derived from mouse peritoneal macrophage cells, were purchased from Korean Cell Line Bank (Seoul, Korea). RAW264.7 cells were maintained in Dulbecco's modified Eagle's medium (DMEM, Hyclon Laboratories, Utah, USA) containing 10% fetal bovine serum (FBS), penicillin 100 IU/mL, and streptomycin 100 μg/mL. Cells were grown in cell culture dish at 37 °C in a 5% CO_2 humidified incubator. In all experiment, the control group was treated with a vehicle (PBS containing 0.5% Pluronic F127) used for dispersion of P-SWCNT, and determined 6.6 μg/mL as the maximum concentration to minimize affect by a vehicle (data not shown).

2.7. Viability analysis

Cell viability was determined using a colorimetric 3-(4-5-dimethylthiazol-2-yl)-2,5-diphenyltetrazolium bromide (MTT, Sigma–Aldrich, St. Louis, MO, USA). Cells (1×10^4 cells/well) were seeded on 96-well plates, stabilized overnight, and then treated with 0.8, 1.6, 3.3 and 6.6 μg/mL (1 μg/cm^2, 7.8×10^{11} fibers/mL) P-SWCNTs for 24 h. After removing the supernatant, the cells were once washed with PBS, PBS containing the MTT solution (200 μL/well) was added to each well, and the cells were incubated for 3 h at 37 °C. Then, the optical density of each well was measured at 540 nm using a microplate spectrophotometer system (VersaMax, Molecular Devices). These data were confirmed using tryphan blue staining method, and the viability of the treated group was expressed as a percentage of the control group (100%).

2.8. Cell cycle analysis

RAW264.7 cells were harvested at 24 h after treatment with the designated concentration of P-SWCNT. After washing, cells were fixed with 70% ethanol, and then cells were stained using propidium iodide and digested with RNase (Sigma–Aldrich). The cell cycle was analyzed by measuring the DNA content using the FACSCalibur system and CellQuest software (BD Biosciences).

2.9. Measurement of ROS and SOD-related trace elements

Reactive oxygen species (ROS) generation was measured using carboxy-2′7′-dichlorodihydrofluorescein diacetate (DCFH-DA, Invitrogen, Carlsbad, CA, USA). Cells were treated with the designated concentration of P-SWCNT for 24 h, and further incubated with 5 μM DCFH-DA at 37 °C for 30 min. Then, cells were

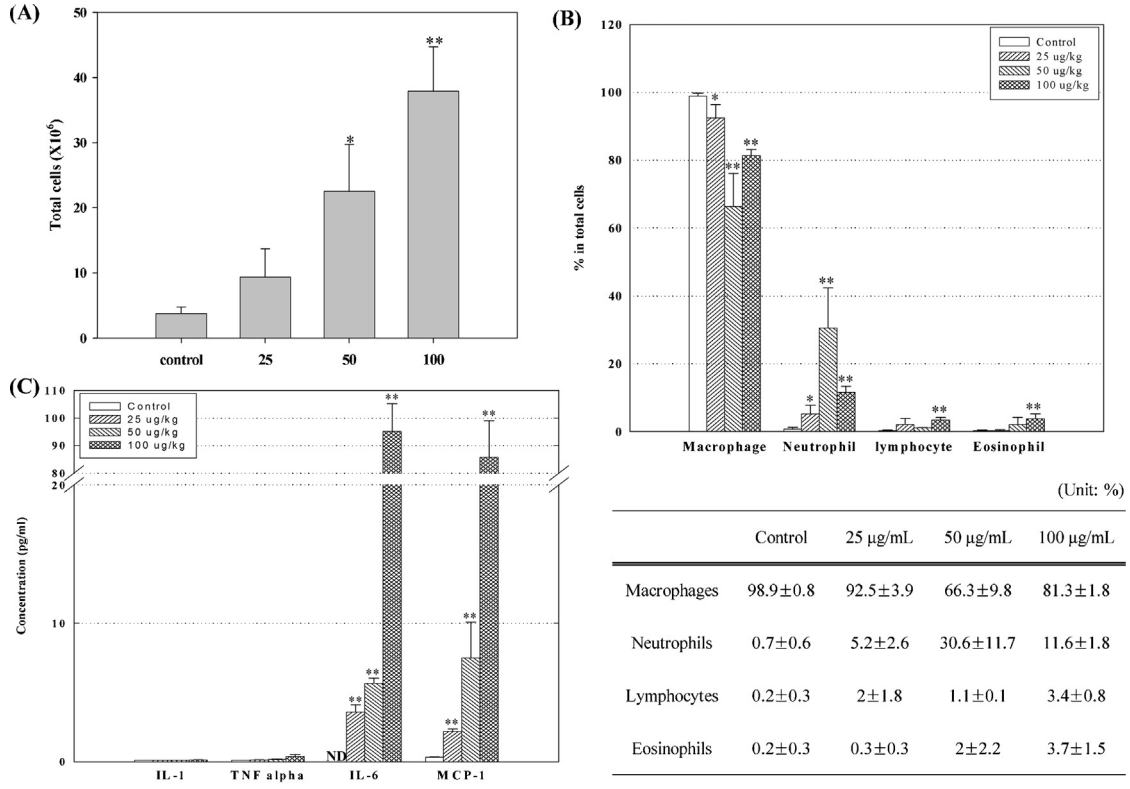

(Unit: %)

	Control	25 μg/mL	50 μg/mL	100 μg/mL
Macrophages	98.9±0.8	92.5±3.9	66.3±9.8	81.3±1.8
Neutrophils	0.7±0.6	5.2±2.6	30.6±11.7	11.6±1.8
Lymphocytes	0.2±0.3	2±1.8	1.1±0.1	3.4±0.8
Eosinophils	0.2±0.3	0.3±0.3	2±2.2	3.7±1.5

Fig. 1. Effect of P-SWCNTs administered intratracheally into lung of mice. BAL fluids ($n = 5$ mice/group) and lung tissues ($n = 4$ mice/group) were harvested at 24 h after a single intratracheal administration. $^*p < 0.05$, $^{**}p < 0.01$. (A) Increase of total cells, (B) differentiation of total cells, (C) changes of cytokines in BAL fluid. Standard curve was made by a serial dilution from blank to 500 pg/mL. (D) Hispathological changes. Black arrows indicate pigmented and foamy macrophages, and red arrow indicates neutrophil infiltration. (For interpretation of the references to colour in this figure legend, the reader is referred to the web version of this article.)

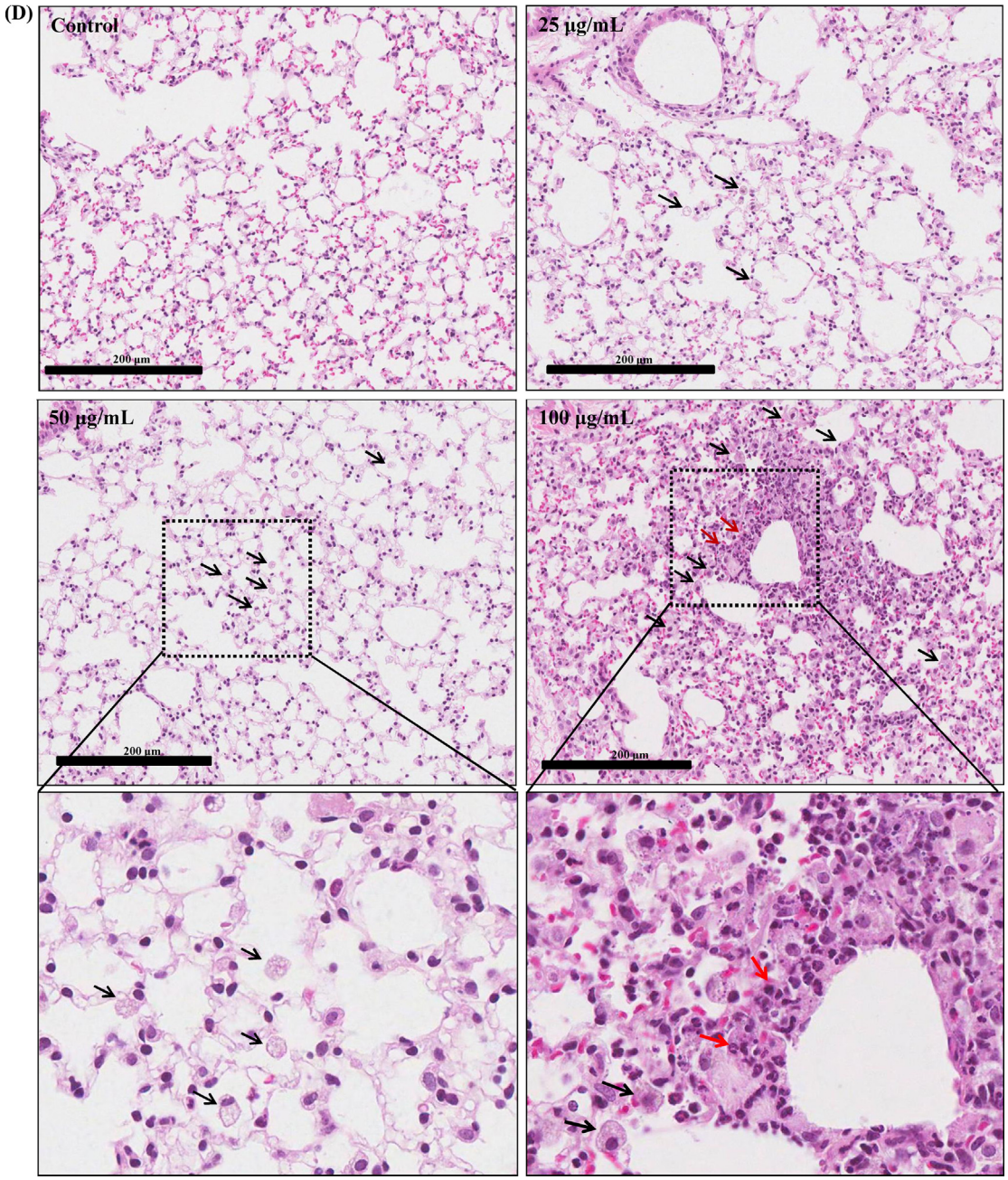

Fig. 1. (Continued)

washed with PBS, and suspended with FBS free DMEM media. Fluorescent cells were counted using the FACSCalibur system and CellQuest software (BD Biosciences). In addition, we measured the level of an antioxidant, superoxide dismutase-related trace element in cells (Park et al., 2014a). At 24 h after exposure, adherent cells were harvested, and re-suspended with PBS (1 mL). Then, cells (500 μL) were digested in a mixed solution of HNO_3 (70%) and H_2O_2 (30%) by using a microwave digestion system (Milestone) under high temperature and pressure. The concentrations of chemicals in lysates were determined using ICP-MS (7700, Agilent) in Korean Basic Science Institute (Seoul, Korea).

2.10. Nitric oxide analysis

Cells (1×10^6 cells/mL) were seeded in a 96-well plate with or without P-SWCNT and incubated for 24 h. The supernatant of 100 μL from each well was transferred to a new 96-well plate, and tested using a nitric oxide (NO) detection kit (iNtRON Biotech, Gyeonggi-do, Korea). The same experiment was performed without cells to exclude the effect of P-SWCNT on the absorbance (Belyanskaya et al., 2007; Kroll et al., 2009). The values were calculated by measuring the absorbance at 540 nm using the microplate spectrophotometer system (VersaMax, Molecular Devices).

2.11. ATP measurement

Cell culture media with or without cells (1×10^4 cells/well) were added in a 96-well plate, and stabilized overnight. P-SWCNT was treated to each well at the designated concentration, and then the plate was incubated for 24 h. At the end of exposure, a volume of CellTiter-Glo® Reagent (Promega, Fitchburg, WI, USA) equal to the volume of cell culture medium present in each well was added,

the contents were mixed for 2 min on an orbital shaker, and further incubated at RT for 10 min. The luminescence value was measured using the microplate luminometer (Berthold Detection Systems, Berthold Technologies GmbH & Co. KG, Bad Wilbad, German).

2.12. Immunohistochemistry

Cells (5000 cells/well) were seeded in two-well chamber slides. After stabilization overnight, cells were incubated without or with P-SWCNT (6.6 μg/mL) for 24 h, and then fixed in 4% paraformaldehyde (PFA) for 15 min at RT. After washing, the cells were fixed again with ice-cold methanol at −20 °C, and then blocked for 1 h using 3% BSA in tris-buffered saline (10 mM Tris, pH 8.0, and 150 mM NaCl) containing 0.05% tween-20 (TBST). Next, the cells were incubated overnight at 4 °C with primary antibodies (1:100 dilution) against p62 (Santa Cruz Biotechnology Inc., Santa Cruz, CA, USA), calnexin (Cell Signaling Technology, Danvers, MA, USA), and lysosome-associated membrane protein (LAMP)-2 (Abcam, Cambridge, MA, USA), and then incubated with Alexa Fluor 488- or 555-conjugated secondary antibodies (1:100 dilution) for 2 h at RT. Mitochondria were labeled with MitoTracker® Deep Red FM (Invitrogen) for 30 min, and the cells were fixed in 4% PFA for 15 min at 37 °C. Coverslips were mounted using Fluoroshield™ mounting medium with DAPI (ImmunoBioScience, Mukilteo, WA, USA), and cells were visualized using a fluorescence confocal laser scanning microscope (LSM710, Carl Zeiss).

2.13. Protein expression

To identify the role of organelle and cellular response according to exposure of P-SWCNT, we investigated changes in protein level as described previously (Park et al., 2014b). Briefly, the equal amounts of protein were separated on polyacrylamide gels and transferred to nitrocellulose membranes (Hybond ECL, Amersham Pharmacia Biotech, Franklin Lakes, NJ, USA). After blocking for 1 h, the membranes were immunoblotted with the following specific primary antibodies (1:1000 dilution): rabbit polyclonal antibodies against poly(ADP-ribose) polymerase (PARP), phospho-p38 (p-p38) and light chain 3B (LC3B, Cell Signaling Technology), beclin 1 and p62 (Santa Cruz Biotechnology), p-IRE 1 alpha and autophagy protein 5 (ATG5, Abcam), and LAMP-2 (Abcam, Cambridge, MA, USA), rabbit monoclonal antibodies against Bcl-2-associated X protein (BAX, Millipore, Milford, MA, USA) and phospho-extracellular signal regulated kinase (p-ERK) and phospho-c-Jun N-terminal kinase (p-JNK, Cell Signaling Technology), mouse monoclonal antibodies against Bcl-2 and cytochorme c (Santa Cruz Biotechnology) and CHOP (Cell Signaling Technology), and goat polyclonal antibody for β-actin (Santa Cruz Biotech). The blots were then incubated with the corresponding conjugated anti-rabbit, anti-mouse or anti-goat immunoglobulin G-horseradish peroxidase (1:2000 dilution, Santa Cruz Biotech). Immunoreactive proteins were detected with the ECL western blotting detection system.

2.14. Morphological changes

RAW264.7 cells were incubated with 6.6 μg/mL P-SWCNT for 24 h. After washing, cells were immediately fixed in 2% glutaraldehyde in 0.1 M sodium cacodylate buffer (pH 7.2) for 2 h. Then, cells were stained for 30 min in 0.5% aqueous uranyl acetate, dehydrated in graded solutions of ethanol, and embedded in spurr's resin. Thin sections were cut on an ultramicrotome (MT-X, RMC, Tucson, AZ, USA), stained with 2% uranyl acetate and Reynolds' lead citrate, and examined in a Carl Zeiss Libra 120 TEM at an accelerating voltage of 80 kV.

2.15. Statistical analysis

Statistical analysis was performed using Student's *t*-test (Graphpad Software, San Diego, CA, USA) and one-way ANOVA test followed by Tukey's post-hoc comparison. Asterisks (*) indicate statistically significant differences with the control group ($^{*}p < 0.05$ and $^{**}p < 0.01$).

3. Results

3.1. Inflammatory response in mice exposed to P-SWCNTs

At 24 h after administration of P-SWCNTs, the numbers of total cells in the BAL fluid increased in a dose-dependent manner, the numbers were 9.4 ± 4.3, 22.5 ± 7.2, and 37.9 ± 6.8 ($\times 10^5$) cells/lung at dosages of 25, 50, and 100 μg/kg, respectively, whereas the number in the control group was 3.8 ± 1.0 ($\times 10^5$) cells/lung (Fig. 1A). As well, the portion of neutrophils significantly increased

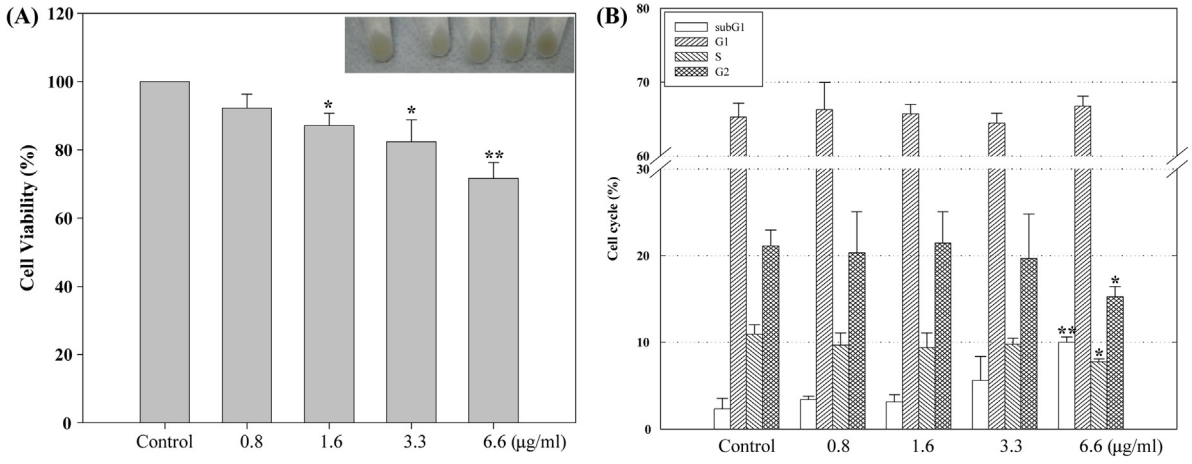

Fig. 2. Effect of P-SWCNTs on cell viability and cell cycle. RAW264.7 cells were exposed for 24 h with the designated concentrations. The experiment was performed four times independently, and results indicate mean ± standard deviation (SD) value. $^{*}p < 0.05$, $^{**}p < 0.01$. (A) Decrease in cell viability. Each experiment was performed using four wells per concentration. Cell viability of the treated group was calculated as a percentage of the control group (100%). Photo shows cells harvested at 24 h after exposure. (B) Changes in cell cycle. A total of 10,000 cells per sample were counted for analysis.

in all treated groups compared to the control group, those of eosinophils and lymphocytes also clearly increased in mice exposed with 100 μg/kg of dose compared to the control group (Fig. 1B). The levels of IL-6 and MCP-1 increased in a dose-dependent manner in the lung after P-SWCNT exposure, but those of IL-1β and TNFα were not detected in all the groups examined (Fig. 1C). The concentrations of IL-6 and MCP-1 were 95.1 ± 10.0 and 85.8 ± 13.2 pg/mL in the 100 μg/kg P-SWCNT group, respectively, whereas these concentrations were not detected and 0.3 ± 0.0 pg/mL in the control group, respectively. Moreover, pigmented macrophages (macrophages that had taken up P-SWCNTs) were observed in the lung tissues of the P-SWCNT-treated groups (Fig. 1D and Supple 2).

3.2. Effect of P-SWCNTs on cell viability and cell cycle in RAW cells

Cell viability decreased in a dose-dependent manner after P-SWCNT exposure (Fig. 2A). When cells were exposed to 0.8, 1.6, 3.3, and 6.6 μg/mL of P-SWCNTs for 24 h, cell viability decreased to 92.2 ± 4.1%, 87.1 ± 3.6%, 82.3 ± 6.5%, and 71.6 ± 4.6% of the control level, respectively. Furthermore, the subG1 proportion, which indicates apoptotic cells, was 3.4 ± 0.4%, 3.2 ± 0.8%, 5.6 ± 2.8%, and 10.0 ± 0.6% in cells treated with 0.8, 1.6, 3.3, and 6.6 μg/mL of P-SWCNTs, respectively, whereas the proportion in the control group was 2.4 ± 1.2% (Fig. 2B). However, cell cycle arrest following P-SWCNT exposure was not observed in any of the treatment groups.

3.3. Changes in cellular components following P-SWCNT exposure

TEM image show that organelle were separated outside the cells due to disappearance of the cell membrane when RAW264.7 cells were exposed with P-SWCNT (Fig. 3A). P-SWCNT also induced the formation of autophagosome-like vacuoles (Fig. 3B), the dilation of the endoplasmic reticulum (ER) (Fig. 3C and D), and the generation of mitochondrial flocculent densities (Fig. 3C, Kamiński et al., 2004). Moreover, the separation of mitochondria from cells (Fig. 4A) and the accumulation of mitochondrial Ca^{2+} (Fig. 4B) were observed in cells exposed to 6.6 μg/mL of P-SWCNTs, and the production of ATP decreased to 67.6 ± 6.3%, 52.6 ± 5.9%, 33.9 ± 4.2%, and 19.1 ± 6.2% of the control level in cells that were exposed to 0.8, 1.6, 3.3, and 6.6 μg/mL of P-SWCNTs, respectively (Fig. 4C). Meanwhile, the LDH level increased slightly relative to control in the cells that were treated with 3.3 μg/mL (104.5 ± 1.0%) and 6.6 μg/mL (107.2 ± 0.8%) of P-SWCNTs (Fig. 4D).

Induction of oxidative stress following P-SWCNT exposure

As shown in Fig. 5A, when cells were exposed to 0.8, 1.6, 3.3, and 6.6 μg/mL of P-SWCNTs for 24 h, the number of cells producing ROS increased to 102.1 ± 1.1%, 124.3 ± 3.9%, 137.9 ± 2.1%, and

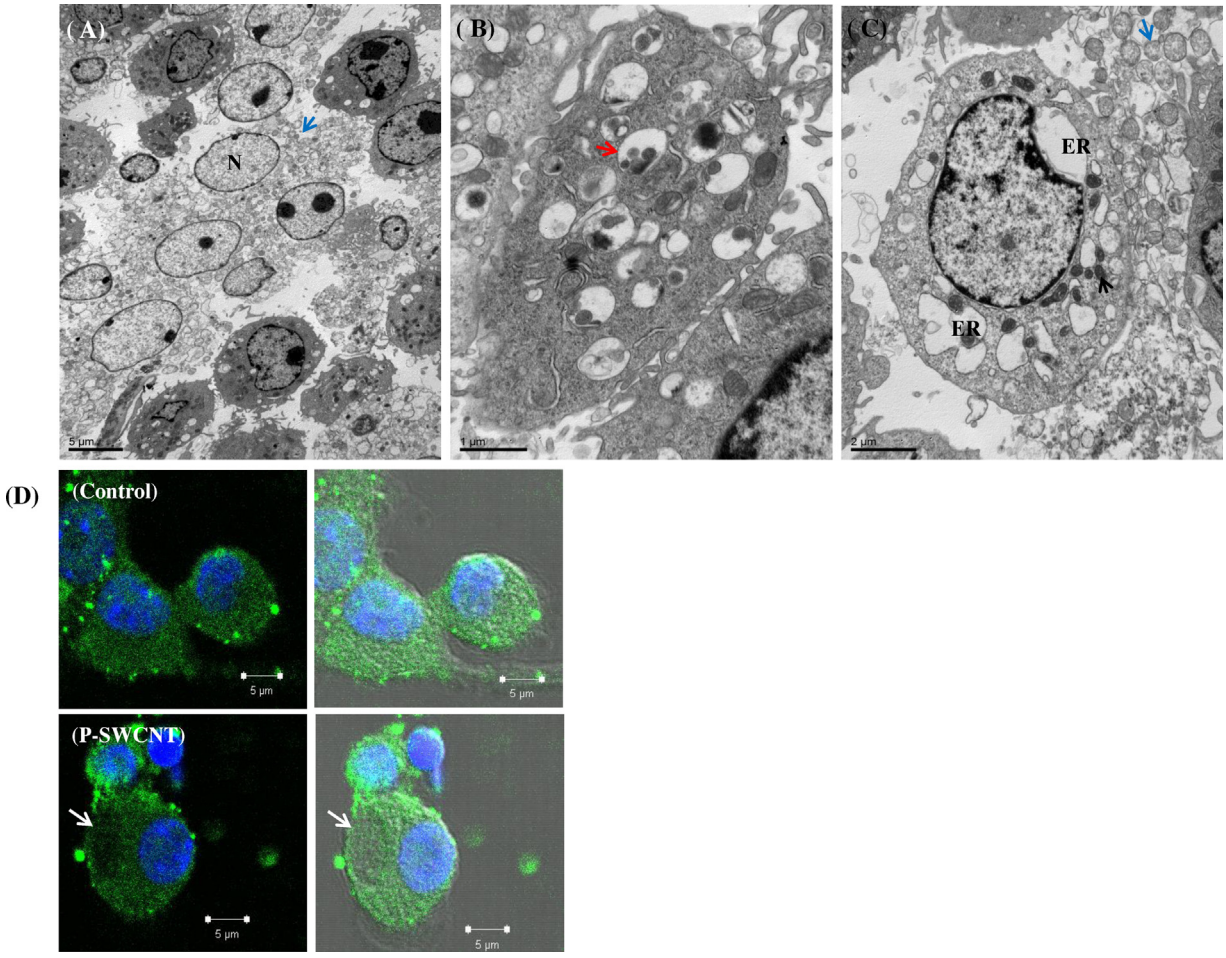

Fig. 3. Morphological changes following P-SWCNT exposure. (A) General image. TEM image was made at 24 h after P-SWCNT exposure (6.6 μg/mL). N: the nucleus, blue arrow indicates the separation of organelle by disappearance of the cell membrane. (B) The increase in autophagosome-like vacuoles (red arrow). (C) Dilatation of the ER and the generation of mitochondria flocculent densities (black arrow). Blue arrow indicates mitochondria separated out of cells. (D) Cells were cultured in the absence or the presence of P-SWCNTs (6.6 μg/mL) for 24 h. The ER was localized by staining calnexin which was embedded in the ER membrane. White arrow indicates the ER swelling. ×800. (For interpretation of the references to colour in this figure legend, the reader is referred to the web version of this article.)

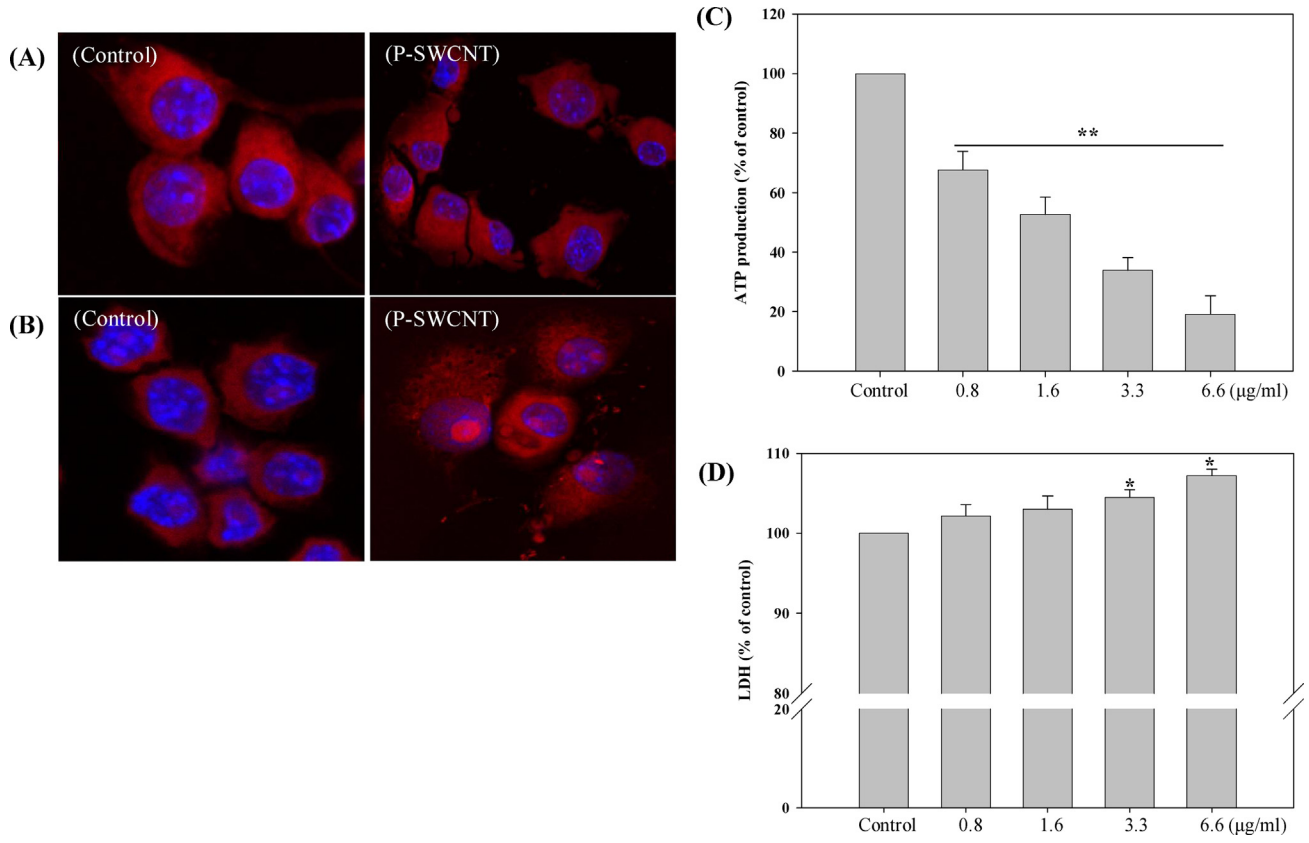

Fig. 4. Damage of cellular components following P-SWCNT exposure. RAW264.7 cells were incubated with or without P-SWCNTs (6.6 μg/mL) for 24 h, and mitochondria (A) and mitochondrial Ca^{2+} (B) were labelled with specific dyes. ×800. (C) Decrease in ATP production. The experiment was performed four times independently, and each experiment was performed using five wells per concentration. Results represent mean ± SD. $^{**}p < 0.01$. (D) Increase of the LDH level. The experiment was performed four times independently, and each experiment was performed using six wells per concentration. Results represent mean ± SD. $^{*}p < 0.05$.

145.1 ± 1.4% of the control level, respectively. Moreover, the NO concentration in the supernatant was 26.2 ± 1.4, 27.4 ± 0.4, 28.8 ± 0.8, and 21.1 ± 2.0 μM in cells treated with 0.8, 1.6, 3.3, and 6.6 μg/mL of P-SWCNTs, respectively, whereas the NO concentration in the control was 4.1 ± 0.3 μM (Fig. 5B). Furthermore, the concentrations of Cu, Zn, and Fe ions increased markedly in cells exposed to P-SWCNTs as compared with their levels in the control (Table 2). However, Mn and Co ions were not detected in any of the samples measured.

3.4. Changes in protein levels following P-SWCNT exposure

As shown in Fig. 6A, the levels of apoptosis-related proteins including BAX, cleaved-PARP, and cytochrome c, and those of autophagy-related proteins such as ATG5, beclin 1, LAMP-2, p62, and LC3B, increased together with the activation of lysosomes after P-SWCNT exposure (Fig. 6B). The p62 was also clearly aggregated in cells treated with 6.6 μg/mL of P-SWCNTs (Fig. 6C). Furthermore, the levels of ER stress-related proteins, such as p-IRE 1 alpha and

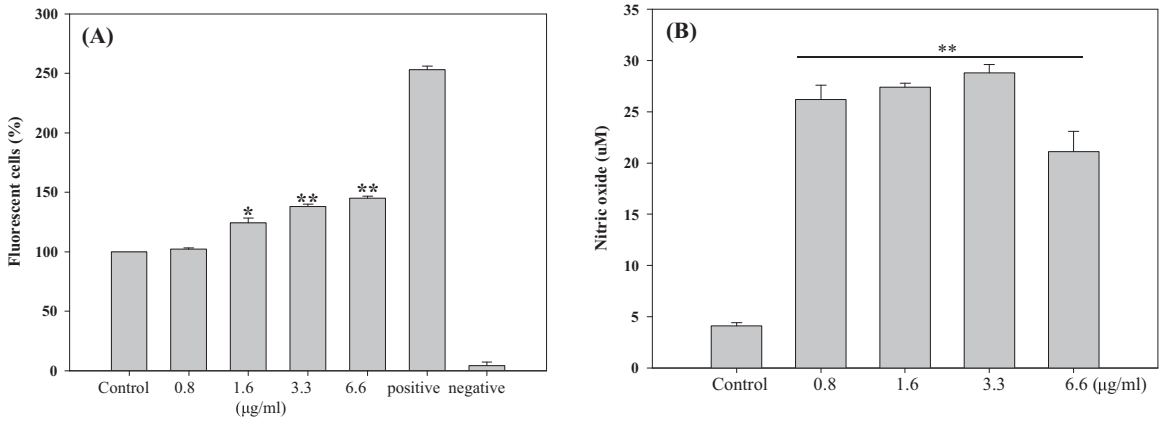

Fig. 5. Generation of ROS and NO following P-SWCNT exposure. The experiment was performed four times independently, and results represent mean ± SD values. $^{*}p < 0.05$, $^{**}p < 0.01$. (A) Increase of cells generating ROS. A total of 10,000 cells per sample were counted for analysis. Negative control was not stained with DCFH-DA, and H_2O_2 (0.03%, positive control) was treated for 1 h. (B) Increase of NO. Each experiment was performed using four wells per concentration, and NO concentration was calculated using a standard curve prepared by a serially diluting $NaNO_2$ (500 μM).

CHOP, increased, and the mitogen-activated protein kinases (MAP Kinases, ERK, p38, and JNK) were activated.

4. Discussion

Nanomaterials are promising materials that have several attractive properties for multiple applications. Occasionally, however, their unique properties play not only as a cause of adverse health effects but also as a limitation in performing the toxicity tests. SWCNTs exhibit hydrophobicity because of the strong van der Waals interaction between nanotubes, and thus the surface of SWCNTs must be modified to improve their dispersibility in hydrophilic solutions used in experiments, especially *in vitro* tests (Nish et al., 2007). In this study, we used a biocompatible surfactant based on a triblock copolymer, Pluronic F127 (Dumortier et al., 2006; Escobar-Chavez et al., 2006). The Pluronic F127 polymer contains propylene oxide (PO) and ethylene oxide (EO) groups. The PO groups wrap the sidewalls of SWCNTs, whereas the EO groups expand into the aqueous phase and create steric repulsion (Mura et al., 2011; Porter et al., 1992). Zhang and Monteiro-Riviere (2009) reported that the non-covalent method of dispersing SWCNTs by the Pluronic F127 polymer is advantageous because it maintains the intrinsic properties of the SWCNT structure.

Concern on health effect of CNTs has been triggered from the possibility of long accumulation in the body due to their high aspect ratio as asbestos (Donaldson et al., 2011). In this study, the proportions of neutrophils and the number of total cells clearly increased along with macrophages taken-up P-SWCNTs in the P-SWCNT-treated groups at 24 h after administration. As well, the levels of IL-6 and MCP-1clearly increased in the lung of mice exposed at a 100 μg/kg of dose together with the portions of eosinophils and lymphocytes. SWCNTs are degraded by myeloperoxidase, an enzyme that is secreted by neutrophils (Kagan et al., 2010). Hypochlorite and eosinophils peroxidase, which is created *in vivo* when the human immune system destroys pathogens, also serves as the main oxidizing agent that can modify and degrade nanotubes in areas of inflammation and within phagosomes (Vlasova et al., 2011; Andón et al., 2013). Additionally, innate immune cells, particularly macrophages and epithelial cells, represent the capacity of immediate reaction to pathogenic stimuli by releasing pro-inflammatory cytokines, such as IL-1β, TNFα, and IL-6, and chemokines, attracting different populations of immune cells into the site of injury (Striz et al., 2014; Mizel, 1989). Among them, IL-6 is secreted by T cells and macrophages to stimulate immune response (Chung, 2001), and MCP-1 is primarily secreted by monocytes, macrophages and dendritic cells to recruits immune cells to the sites of inflammation (Deshmane et al., 2009; Melgarejo et al., 2009). Furthermore, in this study, we used P-SWCNTs that featured a hydrodynamic diameter of 48.4 nm, whereas we used SWCNTs (ASP-100F, purity 60–70 wt%, Hanwha Nanotech, Korea) and semi-SWCNTs (acid-treated ASP-100F) that had hydrodynamic diameters of 0.76 μm and 1 μm, respectively, in our previous studies (Park et al., 2011a,b). In all our studies, the dominance of Th2-type cytokines (Supple 3A) and a relative increase of B and $CD4^+$ T cells (Supple 3B) were observed in the P-SWCNTs-treated groups on Day 28 after a single administration. Meanwhile, the frequency and the level of pigmented macrophages (macrophages that had taken up P-SWCNTs) were higher in this study than in the previous studies (Supple 4). Thus, we hypothesize that SWCNTs are easily taken up by macrophages as their length becomes short (Mutlu et al., 2010), and that SWCNTs may induce similar immune response regardless of their properties. In addition, we used SWCNTs synthesized by conventional arc-discharge process using Fe-based metal catalysis in the previous studies. Thus, we feel that further study needs to compare the chronic health effect of SWCNTs synthesized by different methods under the same experimental conditions.

Inhalation is one of the main exposure routes for nanoparticles, and recognition, tethering, engulfment, and digestion of nanoparticles by macrophages, one of the primary responders to nanoparticles, may be critical for regulating the inflammatory responses and oxidative stress caused by nanoparticles and initiating immune response, as well as for the biodistribution and biodegradation of nanoparticles. In this study, P-SWCNTs reduced cell viability to approximately 71.6% of the control levels in RAW264.7, but they did not induce a notable increase in the LDH level, which is an indicator of necrosis (Chan et al., 2013), although P-SWCNTs clearly caused membrane damage (Supple 5) and markedly lowered ATP production (Kroll et al., 2009). Considering that SWCNTs damaged mitochondrial function through attenuation of electron transfer and the conformational change of cytochrome c (Ma et al., 2012), and that the MTT assay is used to measure mitochondrial function, we hypothesize that a part of the cell death following exposure of P-SWCNTs could be attributed to the effects of Fe, although Fe is essential for mitochondrial function under physiological conditions (Park et al., 2014b). Furthermore, in this study, cells were cultured in media that contained only a small amount of FBS (5.5% when adjust at a 6.6 μg/mL the maximum treatment concentration) because the stock concentration of P-SWCNTs was low (14.58 μg/mL). Therefore, we hypothesize that the decrease in cell viability caused by exposure of P-SWCNTs might be accelerated under starvation (Gülden et al., 2006).

Cell death pathways are functionally categorized as programmed cell death (PCD) and accidental cell death, and apoptosis, autophagy, necroptosis, and paraptosis are representative forms of PCD (Eidi et al., 2012; Khan et al., 2012). Each cell death pathway is also characterized by specific morphological and biochemical changes (Andón and Fadeel 2013; Kroemer and Levine 2008; Galluzzi and Kroemer 2008; Henics and Wheatley 1999; Schwartz et al., 1993; Sperandio et al., 2000; Galluzzi et al., 2012). For example, the formation of vacuoles containing organelles and the generation of an isolation membrane are the key morphological changes that can identify autophagic cell death (Degterev and Yuan 2008; Wu et al., 2012). Apoptosis is indicated by blebbing, chromatin condensation, and fragmentation of the cell and its nucleus and DNA, whereas paraptosis is characterized by cytoplasmic vacuolization and the dilation of mitochondria and the ER. Moreover, apoptosis is controlled by a diverse range of signals, and autophagy is regulated by proteins such as PI3K, mammalian target of rapamycin, the Atg series of proteins, and LC3. Apoptosis, but not paraptosis, involves a cleavage of PARP (Eidi et al., 2012). The p62 protein, which forms aggregates that are degraded by autophagy, acts at the crossroads of autophagy and apoptosis (Trump et al., 1997; Kar et al., 2009), and MAP Kinases, including ERK, JNK, and p38 regulate cell proliferation, gene expression, cell survival, and cell death

Table 2
Changes of SOD-related elements following P-SWCNT exposure RAW264.7 cells were harvested at 24 h after P-SWCNT exposure, and digested in a mixture of HNO_3 (70%) and H_2O_2 (30%) solution using a microwave digestion system under high temperature and pressure. The experiment was performed three times independently.

	Fe	Cu	Zn
Control	6.19 ± 0.32	10.67 ± 0.03	21.15 ± 1.71
0.8	13.05 ± 0.29**	13.55 ± 0.03*	25.46 ± 1.04*
1.7	24.58 ± 2.10**	17.94 ± 0.42**	31.48 ± 0.32**
3.3	28.02 ± 1.95**	17.99 ± 0.33**	32.85 ± 0.17**
6.6	38.64 ± 1.17**	20.65 ± 0.24**	41.70 ± 1.18**

* $p < 0.05$.
** $p < 0.01$.

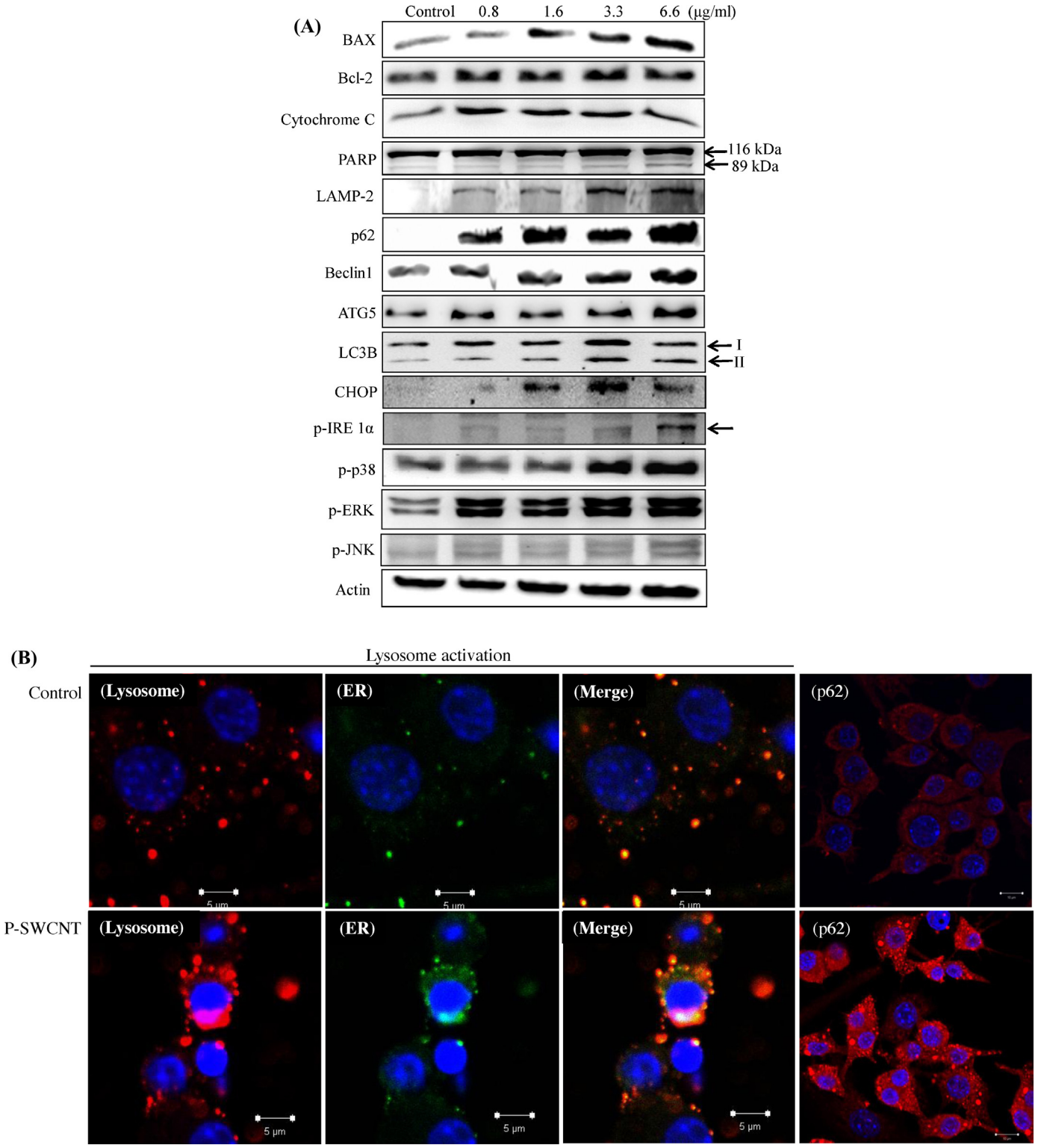

Fig. 6. Changes in protein expression following P-SWCNTs exposure. (A) Changes in cell death-related proteins. The experiment was performed three times independently, and the results showed similar trends. The representative images were presented. (B) Increase of lysosome activity and the aggregated p62. ×800. Cells were incubated in the presence (6.6 μg/mL) or the absence of P-SWCNT for 24 h. Then, cells were co-stained with LAMP-2 (lysosome) and calnexin (ER) and stained with p62 antibody.

pathways (Moscat and Diaz-meco 2009). Furthermore, Ca^{2+} influxes into the mitochondria act as an initial and critical signal in the case of paraptosis, triggering the dilation of both mitochondria and the ER (Eidi et al., 2012; Dodson et al., 2013; Heath-Engel et al., 2012). Some researchers reported that functionalized-SWCNT induced apoptosis or autophagy *in vitro* system (Liu et al., 2011; Dong et al., 2012; Wan et al., 2013; Witasp et al., 2009), and P-SWCNTs also induced autophagic cell death in

our previous study using BEAS-2B cells. Moreover, in this study, P-SWCNTs induced the formation of autophagosome-like vacuoles, increased the levels of autophagy-related proteins, decreased ATP production, and increased the concentration of SOD-1 (cytosolic SOD)-related elements (Cu and Zn), but not of a SOD-2 (mitochondrial SOD)-related element (Mn), in a dose-dependent manner as in BEAS-2B cells. However, the generation of mitochondrial flocculent densities, the extrusion of mitochondria to the outside of the cell, the dilation of ER, and the separation of organelle by disappearance of the cell membrane were observed only in RAW264.7 cells (Noda et al., 2009). P-SWCNTs also induced higher levels of apoptosis in RAW264.7 cells (despite exhibiting lower cytotoxicity) as compared with their effects on BEAS-2B cells. The increased level of ROS was similar between both cells, but the level of NO rather decreased in RAW264.7 cells treated with the maximum concentration (6.6 μ/mL) unlike in the case of BEAS-2B cells. Furthermore, P-SWCNTs increased the level of ER stress-related proteins, enhanced lysosomal activity, and activated MAP Kinases, especially ERK, in RAW264.7 cells. Meanwhile, P-SWCNTs up-regulated the expression of the gene encoding MAP Kinase 8-interacting protein 3 (1.69 fold), which regulates the JNK signaling pathway suppressing ERK pathway (Kuboki et al., 2000), and the expression of the gene encoding BTG family-member 2 (1.67 fold), which controls cell cycle progression at G1 phase (Guardavaccaro et al., 2000), together with cell cycle arrest in G1 phase, in BEAS-2B cells (data not shown). RAW264.7 cells exhibit high lysosomal activity, whereas BEAS-2B cells exhibit low lysosomal activity (Lee et al., 1992, www.atcc.org). Considering that cell death can be initiated in organelles such as mitochondria, the ER, and lysosomes, and that the cell death pathways can intersect under certain intracellular conditions (Ferri and Kroemer 2001; Stern et al., 2012), we feel the need of further study to uncover the roles of organelles in cell death according to exposure of P-SWCNTs.

Based on these results, we suggest that P-SWCNTs induce apoptosis and autophagy through mitochondrial dysfunction and ER stress in RAW264.7 cells, and that instilled P-SWCNTs induce acute inflammatory response. We also feel the need of further study for the relationship between cell death pathways *in vitro* and P-SWCNTs-induced immune responses *in vivo*.

Conflict of interest

The authors report no declarations of interest.

Transparency document

The Transparency document associated with this article can be found in the online version.

Acknowledgements

This work was supported by the Basic Science Research Program through the National Research Foundation of Korea funded by the Ministry of Education, Science and Technology (2011-35B-E00011). And, a part of this research was supported by the National Research Foundation of Korea, the Ministry of Education, Science and Technology (NRF-2010-0020820).

Appendix A. Supplementary data

Supplementary data associated with this article can be found, in the online version, at http://dx.doi.org/10.1016/j.toxlet.2014.06.015.

References

Andón, F.T., Fadeel, B., 2013. Programmed cell death: molecular mechanisms and implications for safety assessment of nanomaterials. Acc. Chem. Res. 46 (3), 733–742.

Andón, F.T., Kapralov, A.A., Yanamala, N., Feng, W., Baygan, A., Chambers, B.J., Hultenby, K., Ye, F., Toprak, M.S., Brandner, B.D., Fornara, A., Klein-Seetharaman, J., Kotchey, G.P., Star, A., Shvedova, A.A., Fadeel, B., Kagan, V.E., 2013. Biodegradation of single-walled carbon nanotubes by eosinophil peroxidase. Small 9 (16), 2721–2729.

Arlt, M., Haase, D., Hampel, S., Oswald, S., Bachmatiuk, A., Klingeler, R., Schulze, R., Ritschel, M., Leonhardt, A., Fuessel, S., Büchner, B., Kraemer, K., Wirth, M.P., 2010. Delivery of carboplatin by carbon-based nanocontainers mediates increased cancer cell death. Nanotechnology 21, 335101.

Belyanskaya, L., Manser, P., Spohn, P., Bruinink, A., Wick, P., 2007. The reliability and limits of the MTT reduction assay for carbon nanotubes-cell interaction. Carbon 45 (13), 2643–2648.

Boczkowski, J., Lanone, S., 2012. Respiratory toxicities of nanomaterials – a focus on carbon nanotubes. Adv. Drug Deliv. Rev. 64 (15), 1694–1699.

Chan, F.K., Moriwaki, K., De Rosa, M.J., 2013. Detection of necrosis by release of lactate dehydrogenase activity. Methods Mol. Biol. 979, 65–70.

Chung, K.F., 2001. Cytokines in chronic obstructive pulmonary disease. Eur. Respir. J. 50s–59s.

Degterev, A., Yuan, J., 2008. Expansion and evolution of cell death programmes. Nat. Rev. Mol. Cell Biol. 9 (5), 378–390.

Deshmane, S.L., Kremlev, S., Amini, S., Sawaya, B.E., 2009. Monocyte chemoattractant protein-1 (MCP-1): an overview. J. Interferon Cytokine Res. 29 (6), 313–326.

Dodson, M., Darley-Usmar, V., Zhang, J., 2013. Cellular metabolic and autophagic pathways: traffic control by redox signaling. Free Radic. Biol. Med. 63, 207–221.

Donaldson, K., Murphy, F., Schinwald, A., Duffin, R., Poland, C.A., 2011. Identifying the pulmonary hazard of high aspect ratio nanoparticles to enable their safety-by-design. Nanomedicine (Lond) 6, 143–156.

Dong, P.X., Wan, B., Guo, L.H., 2012. In vitro toxicity of acid-functionalized single-walled carbon nanotubes: effects on murine macrophages and gene expression profiling. Nanotoxicology 6 (3), 288–303.

Dumortier, G., Grossiord, J.L., Agnely, F., Chaumeil, J.C., 2006. A review of poloxamer 407 pharmaceutical and pharmacological characteristics. Pharm. Res. 23, 2709–2728.

Eidi, H., Joubert, O., Némos, C., Grandemange, S., Mograbi, B., Foliguet, B., Tournebize, J., Maincent, P., Le Faou, A., Aboukhamis, I., Rihn, B.H., 2012. Drug delivery by polymeric nanoparticles induces autophagy in macrophages. Int. J. Pharm. 422 (1-2), 495–503.

Escobar-Chavez, J.J., Lopez-Cervantes, M., Naik, A., Kalia, Y.N., Quintanar-Guerrero, D., Ganem-Quintanar, A., 2006. Applications of thermo-reversible pluronic F-127 gels in pharmaceutical formulations. J. Pharm. Pharm. Sci. 9, 339–358.

Ferri, K.F., Kroemer, G., 2001. Organelle-specific initiation of cell death pathways. Nat. Cell Biol. 3 (11), E255–E263.

Gülden, M., Dierickx, P., Seibert, H., 2006. Validation of a prediction model for estimating serum concentrations of chemicals which are equivalent to toxic concentrations in vitro. Toxicol. In Vitro 20 (7), 1114–1124.

Galluzzi, L., Kroemer, G., 2008. Necroptosis: a specialized pathway of programmed necrosis. Cell 135 (7), 1161–1163.

Galluzzi, L., Vitale, I., Abrams, J.M., Alnemri, E.S., Baehrecke, E.H., Blagosklonny, M.V., et al., 2012. Molecular definitions of cell death subroutines: recommendations of the Nomenclature Committee on Cell Death 2012. Cell Death Differ. 19 (1), 107–120.

Guardavaccaro, D., Corrente, G., Govone, F., Micheli, L., D'Agnano, I., Starace, G., et al., 2000. Arrest of G(1)-S progression by the p53-inducible gene PC3 is Rb dependent and relies on the inhibition of cyclin D1 transcription. Mol. Cell Biol. 20 (5), 1797–1815.

Gulati, N., Gupta, H., 2012. Two faces of carbon nanotube: toxicities and pharmaceutical applications. Crit. Rev. Ther. Drug Carrier Syst. 29 (1), 65–88.

Heath-Engel, H.M., Wang, B., Shore, G.C., 2012. Bcl2 at the endoplasmic reticulum protects against a Bax/Bak-independent paraptosis-like cell death pathway initiated via p20Bap31. Biochim. Biophys. Acta 1823 (2), 335–347.

Henics, T., Wheatley, D.N., 1999. Cytoplasmic vacuolation, adaptation and cell death: a view on new perspectives and features. Biol. Cell 91 (7), 485–498.

Kagan, V.E., Tyurina, Y.Y., Tyurin, V.A., Konduru, N.V., Potapovich Al, Osipov, A.N., Kisin, E.R., Schwegler-Berry, D., Mercer, R., Castranova, V., Shvedova, A.A., 2006. Direct and indirect effects of single walled carbon nanotubes on RAW264.7 macrophages: role of iron. Toxicol. Lett. 165 (1), 88–100.

Kagan, V.E., Konduru, N.V., Feng, W., Allen, B.L., Conroy, J., Volkov, Y., et al., 2010. Carbon nanotubes degraded by neutrophil myeloperoxidase induce less pulmonary inflammation. Nat. Nanotechnol. 5, 354–359.

Kamiński, M., Niemczyk, E., Masaoka, M., Karbowski, M., Hallmann, A., Kedzior, J., Majczak, A., Knap, D., Nishizawa, Y., Usukura, J., Woźniak, M., Klimek, J., Wakabayashi, T., 2004. The switch mechanism of the cell death mode from apoptosis to necrosis in menadione-treated human osteosarcoma cell line 143B cells. Microsc. Res. Tech. 64 (3), 255–258.

Kar, R., Singha, P.K., Venkatachalam, M.A., Saikumar, P., 2009. A novel role for MAP1LC3 in nonautophagic cytoplasmic vacuolation death of cancer cells. Oncogene 28 (28), 2556–2568.

Khan, M.I., Mohammad, A., Patil, G., Naqvi, S.A., Chauhan, L.K., Ahmad, I., 2012. Induction of ROS, mitochondrial damage and autophagy in lung epithelial cancer cells by iron oxide nanoparticles. Biomaterials 33 (5), 1477–1488.

Kroemer, G., Levine, B., 2008. Autophagic cell death: the story of a misnomer. Nat. Rev. Mol. Cell Biol. 9 (12), 1004–1010.
Kroll, A., Pillukat, M.H., Hahn, D., Schnekenburger, J., 2009. Current in vitro methods in nanoparticle risk assessment: limitations and challenges. Eur. J. Pharm. Biopharm. 72 (2), 370–377.
Kuboki, Y., Ito, M., Takamatsu, N., Yamamoto, K.I., Shiba, T., Yoshioka, K., 2000. A scaffold protein in the c-Jun NH2-terminal kinase signaling pathways suppresses the extracellular signal-regulated kinase signaling pathways. J. Biol. Chem. 275 (51), 39815–39818.
Lam, C.W., James, J.T., McCluskey, R., Arepalli, S., Hunter, R.L., 2006. A review of carbon nanotube toxicity and assessment of potential occupational and environmental health risks. Crit. Rev. Toxicol. 36, 189–217.
Lamm, M.H., Ke, P.C., 2010. Cell trafficking of carbon nanotubes based on fluorescence detection. Methods Mol. Biol. 625, 135–151.
Lee, H.K., Jones, R.T., Myers, R.A., Marzella, L., 1992. Regulation of protein degradation in normal and transformed human bronchial epithelial cells in culture. Arch. Biochem. Biophys. 296 (1), 271–278.
Liu, H.L., Zhang, Y.L., Yang, N., Zhang, Y.X., Liu, X.Q., Li, C.G., Zhao, Y., Wnag, Y.G., Zhang, G.G., Yang, P., Guo, F., Sun, Y., Jiang, C.Y., 2011. A functionalized single-walled carbon nanotube-induced autophagic cell death in human lung cells through Akt-TSC2-mTOR signaling. Cell Death Dis. 2, e159.
Ma, X., Zhang, L.H., Wang, L.R., Xue, X., Sun, J.H., Wu, Y., Zou, G., Wu, X., Wang PC&lt, Wamer, W.G., Yin, J.J., Zheng, K., Liang, X.J., 2012. Single-walled carbon nanotubes alter cytochrome c electron transfer and modulate mitochondrial function. Nano ACS 6 (12), 10486–10496.
Manke, A., Wang, L., Rojanasakul, Y., 2013. Pulmonary toxicity and fibrogenic response of carbon nanotubes. Toxicol. Mech. Methods 23 (3), 196–206.
Melgarejo, E., Medina, M.A., Sánchez-Jiménez, F., Urdiales, J.L., 2009. Monocyte chemoattractant protein-1: a key mediator in inflammatory processes. Int. J. Biochem. Cell. Biol. 41 (5), 998–1001.
Mizel, S.B., 1989. The interleukins. FASEB J. 3 (12), 2379–2388.
Moscat, J., Diaz-meco, M.T., 2009. p62 at the crossroads of autophagy, apoptosis, and cancer. Cell 137 (6), 1001–1004.
Mura, S., Hillaireau, H., Nicolas, J., Le Droumaguet, B., Gueutin, C., Zanna, S., Tsapis, N., Fattal, E., 2011. Influence of surface charge on the potential toxicity of PLGA nanoparticles towards Calu-3cells. Int. J. Nanomedicine 6, 2591–2605.
Mutlu, G.M., Budinger, G.R., Green, A.A., Urich, D., Soberanes, S., Chiarella, S.E., Alheid, G.F., McCrimmon, D.R., Szleifer, I., Hersam, M.C., 2010. Biocompatible nanoscale dispersion of single-walled carbon nanotubes minimizes in vivo pulmonary toxicity. Nano Lett. 10 (5), 1664–1670.
Nel, A.E., Mädler, L., Velegol, D., Xia, T., Hoek, E.M., Somasundaran, P., Klaessig, F., Castranova, V., Thompson, M., 2009. Understanding biophysicochemical interactions at the nano-bio interface. Nat. Mater. 8 (7), 543–557.
Nish, A., Hwang, J.Y., Doig, J., Nicholas, R.J., 2007. Highly selective dispersion of single-walled carbon nanotubes using aromatic polymers. Nat. Nanotechnol. 2 (10), 640–646.
Noda, T., Fujita, N., Yoshimori, T., 2009. The late stages of autophagy: how does the end begin? Cell Death Differ. 16 (7), 984–990.
Park, E.J., Roh, J., Kim, S.N., Kang, M.S., Han, Y.A., Kim, Y., Hong, J.T., Choi, K., 2011a. A single intratracheal instillation of single-walled carbon nanotubes induced early lung fibrosis and subchronic tissue damage in mice. Arch. Toxicol. 85, 1121–1131.
Park, E.J., Roh, J., Kim, S.N., Kang, M.S., Lee, B.S., Kim, Y., Choi, S., 2011b. Biological toxicity and inflammatory response of semi-single-walled carbon nanotubes. PLoS One 6, e25892.
Park, E.J., Umh, H.N., Kim, S.W., Cho, M.H., Kim, J.H., Kim, Y., 2014b. ERK pathway is activated in bare-FeNPs-induced autophagy. Arch. Toxicol. 88 (2), 323–336.
Park, E.J., Zahari, N.E., Lee, E.W., Song, J., Lee, J.H., Cho, M.H., et al., 2014. SWCNTs induced autophagic cell death in human bronchial epithelial cells. Toxicol. In Vitro 28 (3), 442–450.
Porter, C.J., Moghimi, S.M., Illum, L., Davis, S.S., 1992. The polyoxyethylene/polyoxypropylene block co-polymer poloxamer-407 selevtively redirects intravenously injected microspheres to sinusoidal endothelial cells of rabbit bone marrow. FEBS Lett. 305, 62–66.
Prato, M., Kostarelos, K., Bianco, A., 2008. Functionalized carbon nanobutes in drug design discovery. Acc. Chem. Res. 41, 60–68.
Rösner, B., Guldi, D.M., Chen, J., Minett Al, Fink, R.H., 2014. Dispersion and characterization of arc discharge single-walled carbon nanotubes-towards conducting transparent films. Nanoscale 6 (7), 3695–3703.
Saito, N., Usui, Y., Aoki, K., Narita, N., Shimizu, M., Hara, K., Ogiwara, N., Nakamura, K., Ishigaki, N., Kato, H., Taruta, S., Endo, M., 2009. Carbon nanotubes: biomaterial applications. Chem. Soc. Rev. 38, 1897–1903.
Saptarshi, S.R., Duschl, A., Lopata, A.L., 2013. Interaction of nanoparticles with proteins: relation to bio-reactivity of the nanoparticle. J. Nanobiotechnol. 11, 26.
Schwartz, L.M., Smith, S.W., Jones, M.E., Osborne, B.A., 1993. Do all programmed cell deaths occur via apoptosis? Proc. Natl. Acad. Sci. U.S.A. 90 (3), 980–984.
Sperandio, S., de Belle, Bredesen, D.E., 2000. An alternative, nonapoptotic form of programmed cell death. Proc. Natl. Acad. Sci. U. S. A. 97 (26), 14376–14381.
Stern, S.T., Adiseshaiah, P.P., Crist, R.M., 2012. Autophagy and lysosomal dysfunction as emerging mechanisms of nanomaterial toxicity. Part. Fibre Toxicol. 9, 20.
Striz, I., Brabcova, E., Kolesar, L., Sekerkova, A., 2014. Cytokine networking of innate immunity cells: a potential target of therapy. Clin. Sci. (Lond). 126 (9), 593–612.
Trump, B.F., Berezesky, I.K., Chang, S.H., Phelps, P.C., 1997. The pathways of cell death: oncosis, apoptosis, and necrosis. Toxicol. Pathol. 25 (1), 82–88.
Usui, Y., Aoki, K., Narita, N., Murakami, N., Nakamura, I., Nakamura, K., Ishigaki, N., Yamazaki, H., Horiuchi, H., Kato, H., Taruta, S., Kim, Y.A., Endo, M., Saito, N., 2008. Carbon nanotubes with high bone-tissue compatibility and bone-formation acceleration effects. Small 4, 240–246.
Vlasova, I.I., Sokolov, A.V., Chekanov, A.V., Kostevich, V.A., Vasil'ev, V.B., 2011. Myeloperoxidase-induced biodegradation of single-walled carbon nanotubes is mediated by hypochlorite. Bioorg. Khim. 37, 510–521.
Walkey, C.D., Chan, W.C., 2012. Understanding and controlling the interaction of nanomaterials with proteins in a physiological environment. Chem. Soc. Rev. 41 (7), 2780–2799.
Wan, B., Wang, Z.X., Ly, Q.Y., Dong, P.X., Zhao, L.X., Yang, Y., Guo, L.H., 2013. Single-walled carbon nanotubes and graphene oxides induce autophagosome accumulation and lysosome impairment in primarily cultured murine peritoneal macrophages. Toxicol. Lett. 221 (2), 118–127.
Wang, J., Sun, P., Bao, Y., Dou, B., Song, D., Li, Y., 2012. Vitamin E renders protection to PC12cells against oxidative damage and apoptosis induced by single-walled carbon nanotubes. Toxicol. In Vitro 26 (1), 32–41.
Witasp, E., Shvedova, A.A., Kagan, V.E., Fadeel, B., 2009. Single-walled carbon nanotubes impair human macrophage engulfment of apoptotic cell corpses. Inhal. Toxicol. 21 (Suppl. 1), 131–136.
Wu, W., Liu, P., Li, J., 2012. Necroptosis: an emerging form of programmed cell death. Crit. Rev. Oncol. Hematol. 82 (3), 249–258.
Zhang, L.W., Monteiro-Riviere, N.A., 2009. Mechanisms of quantum dot nanoparticle cellular uptake. Toxicol. Sci. 110, 138–155.
de la Zerda, A., Kim, J.W., Galanzha, E.I., Gambhir, S.S., Zharov, V.P., 2011. Advanced contrast nanoagents for photoacoustic molecular imaging, cytometry, blood test and photothermal theranostics. Contrast Media Mol. Imaging 6, 346–369.